Ⅰ Ⅰ Ⅰ

(1/3)

NSC94-2120-M009-016-
94 08 01 ～ 95 07 31

(　　)

95　6　1

本計畫第一年主要針對有機化學氣相磊晶系統（MOCVD system）所成長的氮化鋁鎵薄膜表面上微結構作一系列的近場光譜分析。氮化鋁鎵薄膜成長於不同材料的緩衝層（buffer layer）上，因薄膜所受的應力不同， 表面會形成形貌相異之微結構。不同類型的六角丘狀(Hexagonal hillock) 結構出現於以氮化鋁作緩衝層的樣品上。針對不同類型的六角丘狀結構和平坦處比較，譜峰位置會有紅移，之前已有論文指出這現象是因不同的鋁組成分佈所造成的。然而，從近場光譜分析可知，隨著不同類型的六角丘狀結構，其光學特性和其表面形貌也有其特殊的相關性。本計劃中利用近場光學顯微鏡(NSOM)針對單一不同形貌六角丘狀結構以作光學性質之分析。

關鍵詞: 氮化鋁鎵、近場光學

Abstract

In this article, we analyzed the optical properties of the microstructures on AlGaN films with near-field scanning optical microscopy (NSOM). Different types of hillocks(mesa-like, tent-like, and pyramid-like) appeared on the film with AlN buffer layer.

In the NSOM spectra, the emission from the apexes of hillocks of different types of hillock is red-shifted in comparison with that from the plain surface. It may be due to the fluctuation of Al content.

Since the spatial resolution of NSOM (～100 nm) is capable of observing different regions inside single hillock. The luminescence from various probed regions on different types of hillock reflects their properties in detail.

Keywords: AlGaN、NSOM

二、緣由及目的

Hillocks have been observed in metal organic chemical vapor deposition (MOCVD) grown films[1-3]. The hillocks form when the films are under compressive stress.

The micro-structures on Ⅲ-Ⅴ compound semiconductors surfaces have been widely discussed. These structures are formed spontaneously [4-9] or artificially [10-15], and they all have particular optical and electrical properties.

In this report, special emphasis is put on the study of the correlation between the optical properties and topography of the microstructure. In our previous study, we utilized micro-PL to analyze the properties of hillocks on the AlGaN films. However, the spatial resolution of Micro-PL is 2-3 µm. To achieve better resolution, near-field scanning optical microscopy (NSOM) has been employed. The spatial resolution of our NSOM system is about 100 nm and the mapping technique may provide clear correlation between the emission efficiency and topography.

Thus, we will investigate the different facets or regions on all types of hillocks in the AlGaN films with high-resolution NSOM PL system.
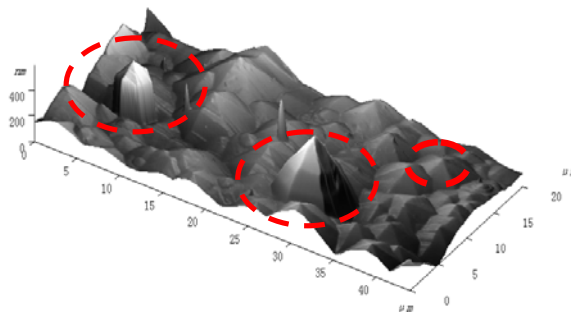
三、結果與討論

Figure 1: 3-D oblique view of three-type Hillocks probed by AFM.

As shown in AFM pictures of Fig.1, there are three types of hillocks on AlGaN sample. The left one called mesa-like hillock, has a quasi-flat top and the angle between the sidewall and the plane region is about 55°. The middle one called tent-like hillock, has two-step sidewall, and the angle between plane region and bottom sidewall is about 22° while the upper sidewall is about 13°. The right one called pyramid-like hillock, is distributed extensively on the sample and the angle between the sidewall and the plane region is about 3°; The size distribution is about 3~5μm and 6~11μm for mesa and tent-like hillocks, respectively. In the report, we will investigate the different facets or regions on all types of hillocks in the AlGaN films with

high-resolution NSOM PL system.

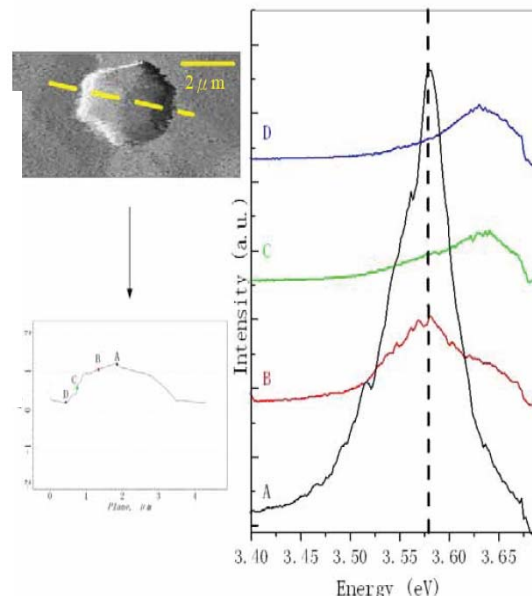3-1 Optical properties of mesa-like hillock

Figure 2: NSOM image, cross-sectional profile, and NSOM PL spectra of one mesa-like hillock. (A, B, C, and D indicate the probed spots.)

Figure 2 shows mesa-like hillock of ～3μm in width and ～0.8μm in height. The NSOM PL spectra were taken at the center, at the middle point between the center and the edge of the quasi-flat facet, on the slope and right on the edge of the mesa-like hillock. Not only the relative intensity but also the peak energy of the emission band differ from the probed regions. I_{NBE} band peaked at 3.623 eV was observed at the edge of the hillock, while the quasi-flat facet is dominated by I_H (3.581 eV) and the intensity deceases rapidly form the center to

the edge. In particular, the PL emission of the slope is dominated by the band peaked at 3.620 eV. It indicates the Al content at the slope may be 2.5 % more than that on the quasi-flat facet, as calculated from Vegard's law

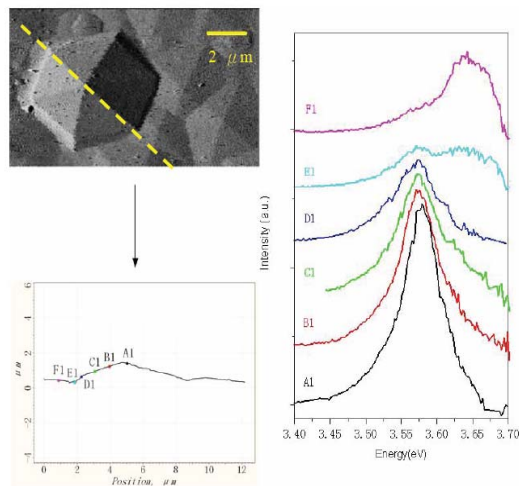## 3-2 optical properties of tent-like hillock

Figure 3 (a) NSOM image, (b) cross-sectional profile along the ridgeline, and (c) NSOM PL spectra of the tent-like hillock. (A1, B1, C1, D1, E1, and F1 indicate the probed spot for PL.)

As we can see from NSOM-PL spectra in Figure 3, the I_H emission band is originated from different positions on the hillock and I_{NBE} is obtained from the edge and the surrounding region, no matter scanning from the apex to the edge along the ridgeline or the slope. The Al composition calculated from the Vegard's law [13] indicated lower Al content (∼8.5 %) on the hillock in comparison with that (∼12 %) from the surrounding region (see Figure 4). The Al concentration is not so different between the ridge and the slope. However, in the intensity mapping images (Figure 5), we can obtain interesting behaviors corresponding to the morphology in detail: (1) The abrupt contrast is shown between the hillock and the surrounding region. When detecting at 340 nm (3.647 eV, the peak of I_{NBE}), the hexagonal dark region can be seen while the emission from the surrounding region is stronger. In contrast, when probing at 347 nm (3.573 eV, the peak of I_H), the emission is mainly from the tent-like hillock. (2) In the intensity profiles, we observe that I_H from the apex is stronger than I_{NBE} in the plain surface by a factor of 2, which is likely due to the localization effect caused by the fluctuation of Al content. Therefore, the carrier excited from the plain region would diffuse to the hillock, where Al content (band gap energy) is less. (3) The ridgeline gives brighter emission than the slope at 347 nm (I_H).
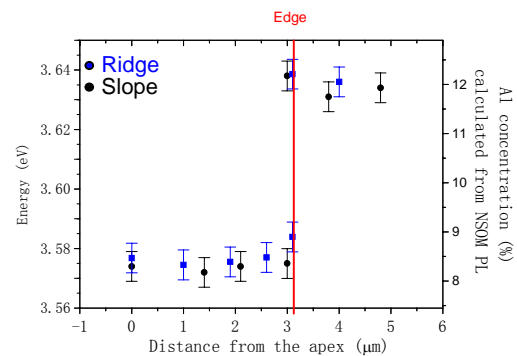

Figure 4: The peak energy and Al concentration profiles along the ridgeline and the slope of the tent-like hillock.
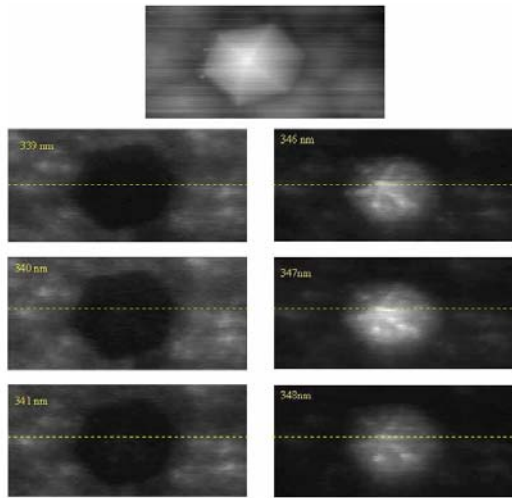
Figure 5:NSOM morphological image (17
μm × 9μm) and NSOM intensity image at
339 nm (3.658 eV), 340 nm (3.647 eV),
341 nm (3.636 eV), 346nm (3.584eV), 347
nm(3.573 eV), and 348 nm(3.563 eV) of
the tent-like hillock.

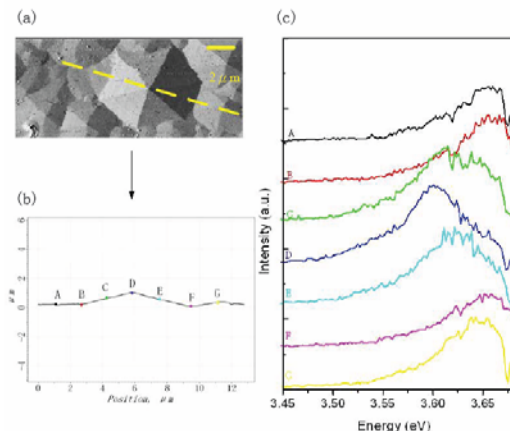## 3-3 optical properties of pyramid -like hillock

Figure 6 (a) NSOM image, (b)
cross-sectional profile, and (c)
NSOM PL spectra of pyramid-like
hillock.

The NSOM morphological image of pyramid -like hillock is shown in Figure 6, We observed one whole pyramid-like hillock, at the center of the image. Its lateral size is about 6μm with 1μm height. We took the NSOM PL spectra from different regions along the line crossing the slope and the apex (Figure 6(b)) of this pyramid-like hillock, as shown in Figure 6(c). The peak energy at the apex is 3.601 eV and is gradually blue-shifted to 3.650 eV when the probed spot is moved from the apex to the edge.

四、結論

We have applied NSOM with higher spatial resolution of ～ 100nm to investigate the correlation between the optical properties and the topography of single hillock in this study. Special emphasis is put on the properties of pyramid-like hillocks (where seem to be the plain region under the optical microscopy of our micro-PL system), the steep slope of the mesa-like hillock, the difference between the apex, slope and ridge on the tent-like hillock.

For the mesa-like hillock, the emission (I_H) from the slope is much weaker and the peak energy is higher than those of the quasi-flat facet. It may be due to the more Al content and high impurity density in the (1-101) facets. For the tent-like hillock, the emission peak did not shift among the various probed regions on the single hillock. Only the intensity showed difference among the different regions. In the intensity-mapping, the apex is the brightest, and the intensity at the

ridgeline is stronger than that from the slopes. For the pyramid-like hillocks, the peak energy increases from the apex to the edge of hillock. The emission peak energy at the apex of different hillocks decreases with the increasing height of hillock or the angle of the slope. We suggested the growth rate in the normal direction increased with the increasing strain caused by lattice misfit between the AlGaN thin film and AlN buffer layer when the film just start to form.

五、參考文獻

1. O. Martinez et al, J. Appl. Phys., 96 3639 (2004)
2. R.Beye et al., Mat. Res. Soc. Proc., 499 113 (1997)
3. L.H. Robins, D.K. Wikenden , Appl. Phys. Lett,. 71 3841 (1997)
4. W. Qian, G. S. Rohrer, M. Skowronski, K.Doverspike, L. B. Rowland, and D. K. GaskillAppl. Phys. Lett. **67** 2284 (1995)
5. Wook Kim, Ö. Aktas, A. E. Botchkarev, A.Salvador, S. N. Mohammad, and H. Morkoç J. Appl. Phys. **79** 7657 (1996)
6. F. A. Ponce, J. W. Steeds, C. D.Dyer and G. D.Pitt Appl. Phys. Lett. **69** (1996)
7. M. Herrera Zaldivar, P. Fernandez, J. Piqueras J. Appl. Phys. **83** 462 (1998)
8. T. H. Myers, L. S. Hirsch, L. T. Romano, and M. R. Richards-Babb J. Vac. Sci. Technol. B **16** 2261 (1998)
9. M. Sumiya, K. Yoshimura, T. Ito, K. Ohtsuka, and S. Fuke, K. Mizuno, M. Yoshimoto, H. Koinuma, A. Ohtomo and M. Kawasaki J. Appl. Phys. **88** 1158 (2000)
10. Koichi Tachibana, Takao Someya, Satomi Ishida, and Yasuhiko Arakawa Appl. Phys. Lett. **76** 3212 (2000)
11. X. Li, P. W. Bohn, Jeongyong Kim, J. O. White, J. J. Coleman Appl. Phys. Lett. **76** 3031 (2000)
12. Kyoyeo Lee, Keunho Auh Jpn. J. Appl. Phys. 40 L 13 (2001)
13. W. Czarczyski, P. Kieszkowski, St. asisz, R. Paszkiewicz, M. Taczaa, Z. Znamirowski, and E. onierz J. Vac. Sci. Technol. B **19** 47 (2001)
14. Yong-Hoon Cho, H. M. Kim, T. W. Kang, J. J. Song ,W. Yang Appl. Phys. Lett. **80** 1141 (2002)
15. HockM. Ng, Nils G. Weimann and Aref Chowdhury J. Appl. Phys. **94** 650 (2003)